Journal of *Marine Science and Engineering*

MDPI

Article

Simulation Study on Methods for Reducing Dynamic Cable Curvature in Floating Wind Power Platforms

Zhitao Guo [1], Xudong Zhao [2], Qingfen Ma [2,*], Jingru Li [2] and Zhongye Wu [2]

[1] POWERCHINA Hainan Electric Power Engineering Co., Ltd., Haikou 570228, China
[2] College of Mechanical and Electrical Engineering, Hainan University, Haikou 570228, China
* Correspondence: mqf0920@hainanu.edu.cn

Abstract: As a key component connecting a floating wind turbine with static sea cables, dynamic cables undergo significant tensile and bending loads caused by hydrostatic pressure, self-weight, waves, and ocean currents during service, which can lead to fatigue failure. Thus, dynamic and fatigue analyses are necessary for the design and operation of dynamic cables. In this study, a fatigue analysis of the three-core four-layer armored dynamic cable used in a semisubmersible floating wind turbine was carried out at a water depth of 25 m. The Miner linear cumulative damage method, based on material S-N curves, was used to predict fatigue life. The results indicate that, at 10 times the safety factor, the dynamic cables meet the design requirement of a 30-year service life in the studied marine environment. The maximal curvature of the dynamic cable always appears at the exit of the bend stiffener, even beyond the allowed point. Adding weights to the section where the cable exits the bend stiffener and adjusting the bend stiffener's hanging angle can both reduce the curvature at the bend stiffener exit. The scheme of adjusting the bend stiffener's hanging angle is preferred, for it is easier for simultaneous adjusting and inducing much smaller extra stress in the cable. As the hanging angle increases, the curvature at the bend stiffener exit decreases, while the maximal effective tension and maximal von Mises stress gradually increase. For certain operating conditions, especially with higher waves, it is better to adjust the hanging angle to avoid excessive curvature and, meanwhile, ensure the increase in the stress within a reasonable range.

Keywords: floating wind power platform; dynamic cable; fatigue analysis; cable curvature; hanging angle

Citation: Guo, Z.; Zhao, X.; Ma, Q.; Li, J.; Wu, Z. Simulation Study on Methods for Reducing Dynamic Cable Curvature in Floating Wind Power Platforms. *J. Mar. Sci. Eng.* **2024**, *12*, 334. https://doi.org/10.3390/jmse12020334

Academic Editor: José António Correia

Received: 20 December 2023
Revised: 5 February 2024
Accepted: 7 February 2024
Published: 15 February 2024

1. Introduction

Against the backdrop of carbon peaking and carbon neutrality goals, the development of power energy is gradually transitioning towards low-carbon directions. As a form of renewable energy, wind power plays a crucial role in the route toward low-carbon transformation of power energy. Offshore wind power, characterized by high utilization hours, zero greenhouse gas emissions, and suitability for large-scale development, is considered a significant pathway for China to achieve its dual carbon goals. In recent years, the development of nearshore fixed wind power platforms has approached saturation [1], while approximately 80% of offshore wind energy resources are distributed in areas with water depths exceeding 60 m [2]. Wind power development is gradually shifting towards deep-sea regions [3,4]. As a system for obtaining wind energy in remote offshore areas, floating offshore wind power platforms are expected to become an inevitable trend in the future development of offshore wind power. The future market scale for dynamic cable systems in the context of floating offshore wind power is projected to reach the hundred-billion level [5–8].

The cable system serves as the conduit for transmitting electrical energy from the floating platform to the onshore location. Based on its operational conditions, the cable system can be categorized into the static cable end and dynamic cable end [9]. The former

primarily refers to conventional submarine cables laid on the seafloor, while the latter is a crucial component of floating offshore wind power platforms, consisting of dynamic cables and their associated accessories [10]. Dynamic cables, serving as the key equipment linking the floating turbine to the static seabed cable, experience significant tensile and bending loads during service due to factors such as water depth pressure, self-weight, waves, and ocean currents. These loads can lead to fatigue failure. Therefore, it is necessary to conduct fatigue performance analyses on the pre-service dynamic cables of floating turbines and predict whether their fatigue life meets the operational requirements.

Current research on fatigue damage of dynamic cables is relatively limited. Relevant studies on flexible risers and umbilical cables with structural and hydrodynamic characteristics similar to dynamic cables can be consulted. Larsen and Passano et al. [11] introduced the principles of frequency domain and time domain methods in fatigue analysis. They conducted fatigue analysis on tensioned risers in the typical North Sea environment, suggesting that the frequency domain method has sufficient accuracy. They also emphasized the importance of considering the combined effects of waves and ocean currents when calculating fatigue life. Hoffman et al. [12,13] proposed a fatigue analysis method based on the Miner fatigue accumulation method, which is applicable to dynamic cables/flexible risers. They considered this method the only feasible approach for handling random stress cycles. Ruan et al. [14] proposed a deepwater-compliant wave-type riser structure based on the arrangement of multiple waveforms in series. They constructed three different riser structures and conducted a dynamic response analysis as well as a fatigue analysis. Guo and Nie et al. [15] proposed a nonlinear contact load calculation method for risers based on elastic–plastic contact collision theory. They established a fatigue life prediction method for experimental risers using the cumulative damage theory. The study analyzed the impact of significant wave height and top tension coefficient on the fatigue life of experimental risers. Lu and Vaz et al. [16] established a nonlinear finite element model for flexible risers with bend stiffeners. They conducted case studies on typical limit and fatigue load scenarios to assess the influence of curvature changes and bend stiffener contact pressure on the stress in the riser armor layer.

Shen G et al. [17] proposed an analytical bending fatigue model for estimating the fatigue life of low-sag cables under harmonic loads and analyzed the effect of the ratio of cable weight to tension on fatigue life. It is found that the curvature and tension of the cable are the main factors affecting the fatigue life of the cable, and the curvature has a greater influence than the tension. Wokem C et al. [18] used finite element modeling techniques to study the stress states of several cables, and the fatigue life of these cables was obtained by combining the stress-based method with the results of finite element modeling. The paper points out that the tension and bending stress of the cable are important factors affecting the fatigue life of the cable, and the fatigue life of the cable is related to the structure and material of the cable. Young et al. [19,20], based on offshore wind power, established a model for dynamic cables to analyze the local stress distribution of the dynamic cable cross-section. They conducted a fatigue damage assessment of the armor wires and insulation materials of dynamic cables through stress time history. The results indicated that bending stress is the primary load causing fatigue damage to dynamic cables. However, the paper did not further investigate how to reduce the curvature of dynamic cables. Excessive local curvature of the cable is one of the main causes of fatigue damage. The curvature at the exit of the bend stiffener is often one of the maximum values. If it exceeds the allowable limit, it will directly exacerbate the fatigue damage to the dynamic sea cable. Currently, the main methods for reducing curvature involve referencing dynamic cables and increasing the weight block [21]. However, there is a lack of research on the influence of the bend stiffener hanging angle on cable curvature and fatigue performance.

This study calculates the stress coefficients of dynamic cables using ABAQUS 2020 software. Based on the professional hydrodynamic analysis software, combined with on-site hydrological data conditions, a time-domain analysis method is employed to conduct fatigue analysis on dynamic cables associated with floating turbines. The Miner linear

cumulative damage method based on material S-N curves is used to predict their fatigue life. This study also investigates the impact of the bend stiffener hanging angle on the fatigue performance of dynamic cables. Based on this, a method to reduce cable curvature by changing the hanging angle is proposed, providing guidance for engineering practice.

2. Fatigue Analysis Method for Dynamic Cables

This paper employs a time-domain analysis method to analyze the fatigue characteristics of dynamic cables. This method takes into account the effects of multiple cyclic loads that dynamic cables experience in actual operational conditions, enhancing the accuracy of the predictive results. It can also be used to assess the fatigue performance of dynamic cables under complex conditions, such as predicting fatigue life under random load conditions. The basic process of time-domain fatigue analysis is illustrated in Figure 1.

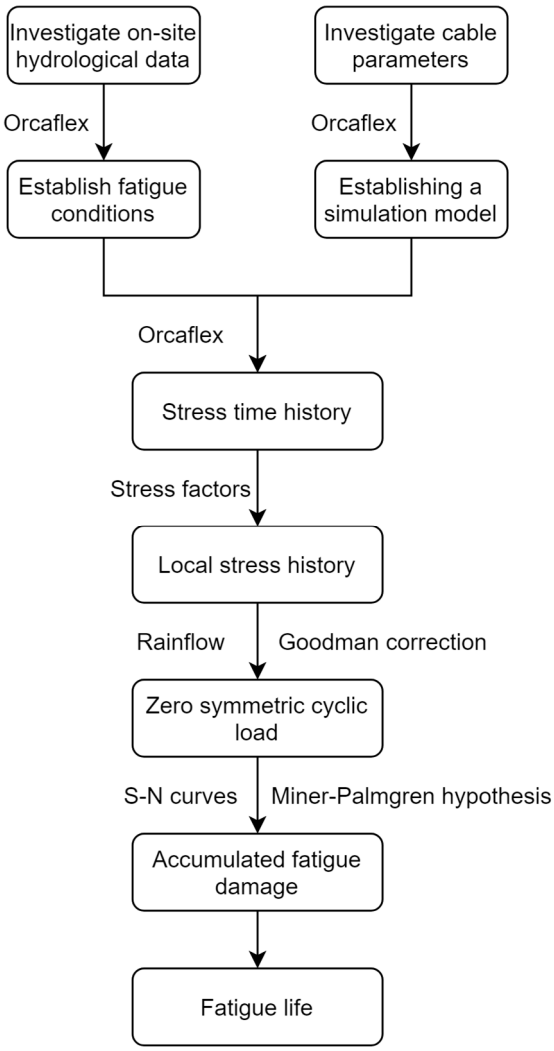

Figure 1. Basic flowchart of time-domain fatigue analysis.

(1) Firstly, it is necessary to clarify the load history experienced by dynamic cables, including external environmental factors (such as wind, waves, and currents) and the loads generated by the cable's vibration. Since dynamic cables are flexible cables with high damping characteristics and are less prone to vortex-induced vibrations, the impact of vortex-induced vibration on the fatigue damage of dynamic cables can be neglected in the line design [22]. When dealing with sea conditions, relevant standards such as IEC 61400-3 [23] and DNV-OS-F201 [24] should be referenced. By referring to measured data, determine the operating conditions the wind turbine

undergoes during its service life. Based on the joint probability distribution table of measured data, a fatigue operating conditions table can be established for different characteristic wave heights, spectral peak periods, directions, and other factors.

(2) Establish a numerical model for the dynamic cable system based on the parameters of the dynamic cable. The model includes the float to which the dynamic cable is connected, the dynamic cable itself, and the necessary accessories for the dynamic cable. The time domain analysis of the dynamic cable is carried out to obtain the stress time history of the dynamic cable at different time points.

(3) Fatigue life prediction for dynamic cables can utilize the stress coefficient method. The dynamic cable is a multi-layer wound structure, and each layer has different material mechanical properties, leading to varying stress coefficients. The main structures include the conductor, insulation, filling, armor wires, and sheath. Among them, the insulation, filling, and sheath are made of polyethylene polymer materials, which generally have a low elastic modulus and high Poisson's ratio, making them less prone to fatigue failure. The focus is primarily on the fatigue damage of the metallic materials in the dynamic cable, such as the conductor and armor wires. Therefore, the stress distribution calculation for the main force-bearing structures, the conductor, and the armor wires in the dynamic cable is carried out through Formula (1) [25].

$$\sigma = K_t T + K_c \left(C_x \sin\theta - C_y \cos\theta \right) \tag{1}$$

where K_t is the effective tension–stress coefficient for the corresponding structure, K_c is the curvature–stress coefficient for the corresponding structure, C_x is the curvature component in the x direction, C_y is the curvature component in the y direction, T is the tension applied to the cable, and θ is the azimuth angle of the fatigue point on the circumference.

(4) The stress time history response obtained above is irregular, and this irregular response can be considered to be composed of a large number of full cycles and half cycles. To further conduct a fatigue life analysis and fatigue load spectrum analysis, the widely used Rain flow counting method in the engineering field is applied to convert the load time response into several load cycles [26]. Through the statistical analysis of the Rain flow counting method, a series of data for full cycles and half cycles are obtained, preparing for the subsequent fatigue analysis.

(5) The several cyclic loads obtained from the Rain flow counting method cannot be directly used for fatigue calculation. During the operation of the dynamic cable, due to the self-weight and motion of the upper floating body, the cable will experience significant tensile loads, resulting in a nonzero average stress. However, the commonly used S-N curve is obtained under conditions of zero-symmetric cyclic loads. Therefore, before using the S-N curve, it is necessary to correct the average stress. Various scholars have proposed different correction methods, such as Goodman, Gerber, Smith–Watson–Topper, etc. Among them, the Goodman correction method [12] is widely applied in engineering practice due to its simplicity. The expression for the corrected stress amplitude is as follows:

$$\sigma_a = \begin{cases} \Delta\sigma / (1 - \sigma_m / \sigma_b), & 0 < \sigma_m < \sigma_b \\ \Delta\sigma, & \sigma_b < \sigma_m < 0 \end{cases} \tag{2}$$

where σ_a is the stress amplitude, $\Delta\sigma$ is the actual stress amplitude, σ_m is the mean stress, and σ_b is the material's ultimate strength limit.

(6) To calculate the fatigue damage value, it is necessary to reference the corresponding material S-N curve. The S-N curve is plotted by subjecting standard material specimens to cyclic loading at different stress amplitudes until failure under a given mean stress condition. The logarithmic form of the S-N curve formula is shown in Equation (3) [25].

$$\log_{10}(N) = \log_{10}(a) - m \log_{10}(\Delta\sigma) \tag{3}$$

where $\log_{10}(a)$ and m are empirical values, which can be determined through relevant standards.

(7) Due to the randomness of the loads, the structure will endure a significant number of corrected stress amplitudes and corresponding stress cycle counts. To obtain the overall fatigue damage of the structure, it is necessary to accumulate damage for each stress state. Currently, the most widely used fatigue accumulation theory in the field of marine engineering is the linear fatigue accumulation method based on the Miner criterion [12]. This method neglects the influence of unordered loading caused by the randomness of the load. Specifically, by comparing the cycle count n_i for each stress state obtained by the Rain flow counting method with the material failure cycle count N_i determined by the S-N curve for that stress amplitude state, the fatigue damage D_i for that stress amplitude can be obtained. The total fatigue damage is then given by D_L:

$$D_L = \sum_{i=1}^{s} \frac{n_i}{N_i} \tag{4}$$

where D_L is the cumulative fatigue damage for all operating conditions, s is the number of fatigue conditions, n_i is the cycle count of the structural stress in the i-th condition, N_i is the number of failures corresponding to the stress amplitude obtained from the S-N curve, and n_i/N_i is the cumulative fatigue damage for the i-th condition. The ultimate fatigue life $F = 1/D_L$ is the reciprocal of the total fatigue damage.

3. Conditions and Characteristics of the Dynamic Cable

Based on a Science and Technology Project of POWERCHINA Hainan Electric Power Engineering Co. Ltd. (Haikou, China), a fatigue analysis was conducted on dynamic cables of the 26/35 kV voltage level. A numerical simulation model of the dynamic cable was established, including the floating platform and dynamic cable. The top end of the dynamic cable was connected to the floating platform with bend stiffeners added at the connection point. The bottom end of the dynamic cable was connected to the static seabed cable laid on the seafloor. The linear shape of the dynamic cable was set as a catenary, and its working water depth was specified as 25 m. To ensure computational accuracy, the grids for the bend stiffener section and float section of the dynamic cable were refined, and the grid accuracy of the section was 0.5 m. The floats are arranged at intervals of 1.5 m from 27 m to 34.5 m of dynamic cable, with a mass of 0.1 t and a volume of 0.23 m^3. The velocity of the flow is in the same direction as the direction of the wave [27]. The hanging angle is 5°. The arrangement of the dynamic cable is illustrated in Figure 2.

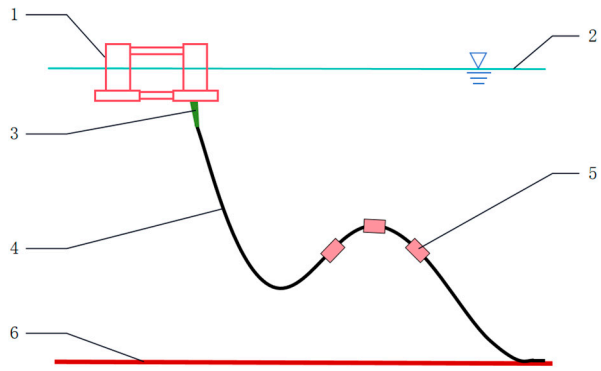

Figure 2. Arrangement of the dynamic cable configuration. 1. Floating platform, 2. sea surface, 3. bend stiffener, 4. dynamic cable, 5. float, 6. seabed.

3.1. Hydrological Conditions

Based on the measured hydrological data in a certain sea area of Hainan Province, tables were established for the probability distribution of significant wave heights in different directions with various characteristic wave heights and directions (Table 1), the

wave conditions (Table 2), and the flow velocity conditions (Table 3). The floating platform adopts a semisubmersible platform; the main scale parameters are shown in Table 4, the geometric parameters are shown in Table 5, and the geometric shape is shown in Figure 3.

Table 1. Probability distribution of significant wave heights in different directions.

Hs(m)\ Direction	N	NE	E	SE	S	SW	W	NW	Subtotal
0.0–0.5	2.49	6.10	13.60	4.84	4.04	6.78	1.78	1.20	40.83
0.5–1.0	4.28	8.98	10.33	0.83	1.13	11.32	0.80	0.10	37.79
1.0–1.5	5.05	2.31	1.07	0.14	0.08	5.06	0.37	0.05	14.14
1.5–2.0	3.46	0.42	0.07	0	0	0.49	0.06	0	4.50
2.0–2.5	1.23	0.10	0.03	0	0	0	0.01	0.046	1.43
2.5–3.0	0.51	0.01	0.02	0	0	0	0	0.046	0.59
3.0–3.5	0.29	0.03	0	0	0	0	0	0.023	0.34
3.5–4.0	0.18	0.01	0	0	0	0	0	0	0.19
4.0–4.5	0.07	0	0	0	0	0	0	0	0.07
4.5–5.0	0.02	0	0	0	0	0	0	0	0.02
5.0–5.5	0.05	0	0	0	0	0	0	0	0.05
5.5–6.0	0.03	0	0	0	0	0	0	0	0.03
>6.0	0.02	0	0	0	0	0	0	0	0.02
Subtotal	17.72	17.97	25.13	5.81	5.25	23.65	3.01	1.46	100
Maximum Value	6.15	3.59	2.71	1.46	1.18	1.82	2.12	3.16	

Table 2. Wave conditions.

Operating Condition	Wave Height (m)	Wave Period (s)	Wave Direction	Wind Speed (m/s)	Wind Direction
100-Year Return Period Wave under 100-Year Return Period High Tide Level	11.8	9.4	NW	40	NW
100-Year Return Period Wave under 100-Year Return Period Low Tide Level	10.62	9.1	NW	40	NW
Multi-Year Average Wave	1.0	3	NE	6	NE

Table 3. Current velocity conditions.

Type	One-Year Return Period Current Velocity (m/s)	Ten-Year Return Period Current Velocity (m/s)	Fifty-Year Return Period Current Velocity (m/s)
Surface Current	1.0	2.0	2.5
Midlayer Current	0.8	1.6	2.0
Near-Bottom Current	0.4	0.7	1.0

Table 4. Floating platform parameters.

Parameters	Values	Parameters	Values		
			X	*Y*	*Z*
Length (m)	103	Centre of gravity (m)	2.53	0	−1.97
Width (m)	15.95				
Molded depth (m)	13.32				
Platform draft (m)	6.66	Moment of inertia tensor (t·m^2)	254.9×10^3	5.980×10^6	5.980×10^6
Mass (t)	9017.95				

Table 5. Floating platform geometry parameters.

Vertices	X (m)	Y (m)	Z (m)
1	53	0	6.66
2	35	8	6.66
3	−50	8	6.66
4	−50	−8	6.66
5	35	−8	6.66
6	40	0	−6.66
7	35	8	−6.66
8	−50	8	−6.66
9	−50	−8	−6.66
10	35	−8	−6.66

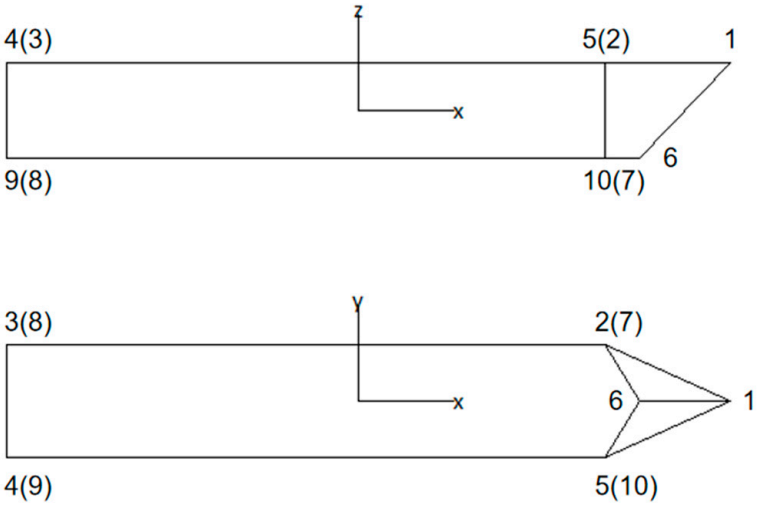

Figure 3. Floating platform geometry.

3.2. Cable Cross-Sectional Structure

The three-core dynamic cable studied in this paper adopts a four-layer armor design. The cross-sectional structure of the cable is shown in Figure 4, and the cable cross-sectional parameters are presented in Table 6.

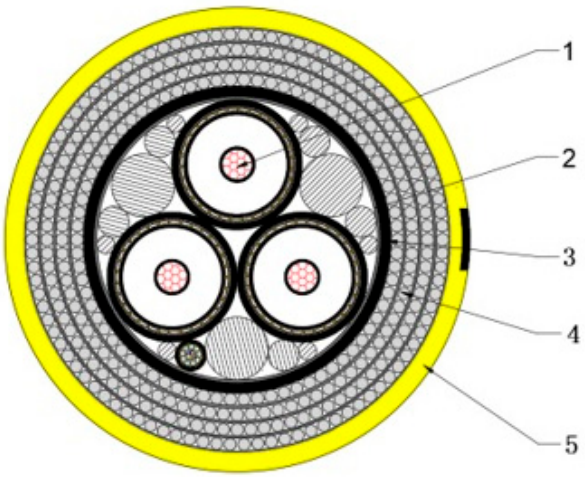

Figure 4. Cross-sectional structure of the cable. 1. Copper conductor, 2. filling, 3. inner sheath, 4. armoring steel wires, 5. outer sheath.

Table 6. Cable cross-sectional parameters.

Parameters	Values	Parameters	Values
Outer Diameter (mm)	147.3	Torsional Stiffness (kN·m^2)	209.8
Dry Weight (kg/m)	45.90 (in air)	Minimum Bending Radius (m)	1.80
Wet Weight (kg/m)	28.43 (underwater)	Minimum Breaking Force (kN)	1351.5
Axial Stiffness (MN)	631.7	Maximum Operating Force (kN)	330.5
Bending Stiffness (kN·m^2)	10.3	Design Lifetime (years)	30

3.3. Selection of S-N Curves

In accordance with the DNV-RP-C203 Fatigue Design of Offshore Steel Structures [28] standard, the values of the empirical constants log(a) and m for the S-N curves of armoring steel wires and copper conductors are provided in Table 7.

Table 7. S-N curve parameters for armoring steel wires and copper conductors.

Structure	log(a)	m
Armoring Steel Wires	14.917	4
Copper Conductors	12.75	3.75

4. Results and Discussion

4.1. Calculation of Local Stress Coefficients

In ABAQUS software, a local model of the dynamic cable was established. Various tensions and moments were applied to obtain the stress distribution of armoring steel wires and copper conductors under different tensions and curvatures. This information was then used to calculate the stress coefficients for the armoring steel wires and copper conductors in the dynamic cable, based on Equation (1). To calculate the stress in specific components of the dynamic cable, it is essential to determine the tension–stress and curvature–stress coefficients for each component.

A finite element local model is established for the dynamic cable to ensure numerical calculation accuracy. The entire model adopts C3D8R elements, which are reduced-integration solid elements. This type of element enhances calculation accuracy while ensuring computational efficiency. The mesh division of the finite element model is shown in Figure 5. During the stretching, bending, and twisting processes of the cable, deformation occurs in each layer, leading to phenomena such as penetration between layers in contact. This can result in a decrease in the accuracy of the calculated results. To prevent these issues, contact between layers needs to be defined. A general contact is applied to the entire model, with normal contact being rigid and tangential contact being free sliding, neglecting the influence of friction. Two reference points are established at both ends of the finite element model, coupled with the corresponding nodes on the cross-section endpoints. The coupling is achieved through continuous distribution coupling at the coupling nodes, where boundary conditions for the finite element model are set. At one end of the model, full constraints are applied to the displacements in all three directions and the rotations in three directions. Additionally, tension loads are applied in the Z-direction at different levels. The stress magnitudes of the armored steel wires and copper conductors under different tensions are obtained. Scatter plots are created based on the tension–stress relationship, and fitting curves are generated, as shown in Figures 6 and 7.

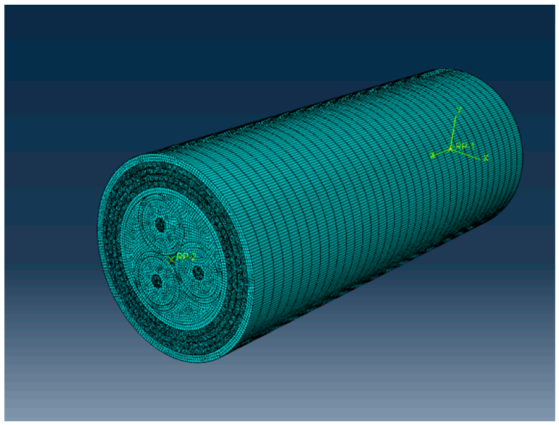

Figure 5. Finite element model of the dynamic cable.

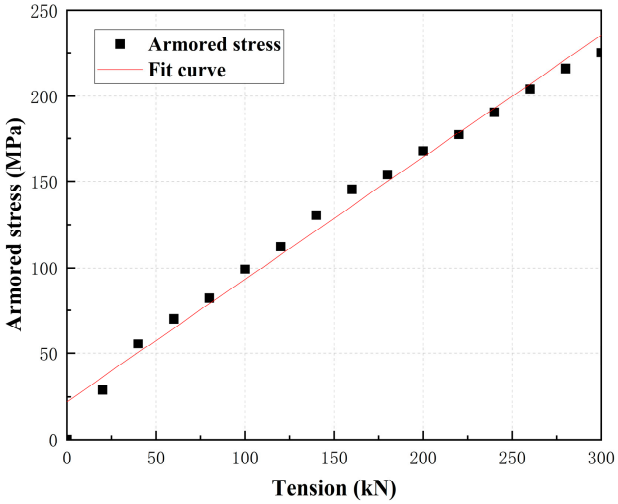

Figure 6. Relationship between tension in armoring steel wires and stress.

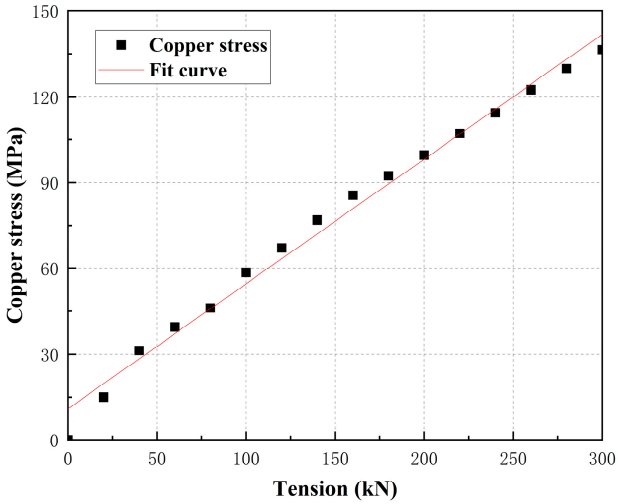

Figure 7. Relationship between tension in copper conductors and stress.

Different moments were applied to the dynamic cable to obtain the stress levels in armoring steel wires and copper conductors under various curvatures. Scatter plots were generated based on the curvature–stress relationship, and fitting curves were derived, as shown in Figures 8 and 9.

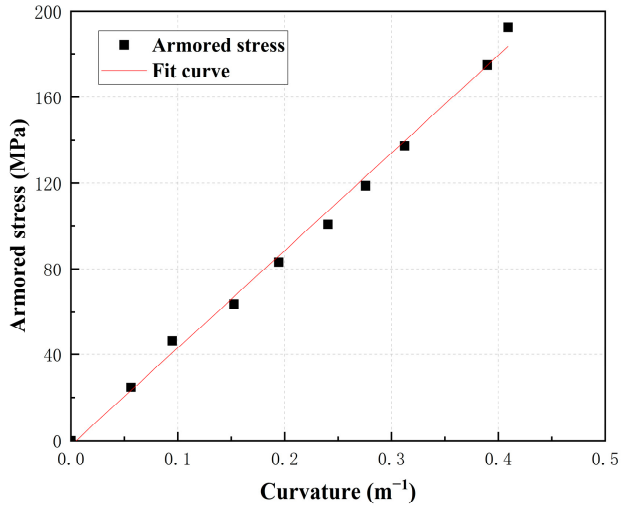

Figure 8. Relationship between curvature in armoring steel wires and stress.

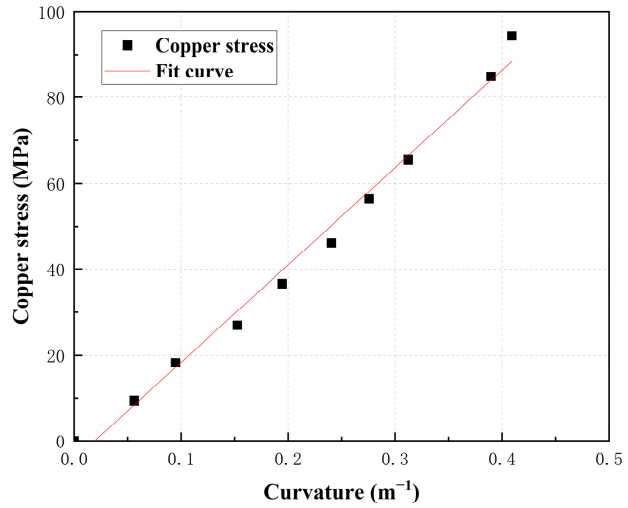

Figure 9. Relationship between curvature in copper conductors and stress.

The scatter plots shown in Figures 6 and 7 can be fitted with lines represented by parameters $y = 0.71119x + 22.057$ and $y = 0.43634x + 10.95$, showing a high degree of alignment. Therefore, the stress generated by the tension in armoring steel wires and copper conductors can be calculated based on these two lines, respectively. Similarly, the scatter plots shown in Figures 8 and 9 can be fitted with lines represented by parameters $y = 454.249x - 2.268$ and $y = 226.784x - 4.349$. When subjected to bending, the stress generated in armoring steel wires and copper conductors can also be calculated based on these two lines. Therefore, the slope of the fitting curves in Figures 6 and 7 represents the tensile stress coefficient K_t of the armored steel wire and the copper conductor, and the slope of the fitting curve in Figures 8 and 9 represents the curvature stress coefficient K_c of the armored steel wire and the copper conductor.

4.2. Results

By processing the long-term sea conditions, the probability of each wave condition was obtained. Combining the probabilities of wave direction and current speed, the probability of wave–current combination conditions was determined. Subsequently, a 3-h time domain analysis was conducted for each combination condition. The fatigue damage values generated by each condition were multiplied by the probability of condition occurrence to obtain the probability of damage for each condition. Finally, these probability

damage values were accumulated to determine the fatigue damage for the long-term sea conditions. The results are shown in Figure 10. According to the DNV-ST-F201 specification, the safety factor is 10, and the dynamic cable meets the design life of 30 years.

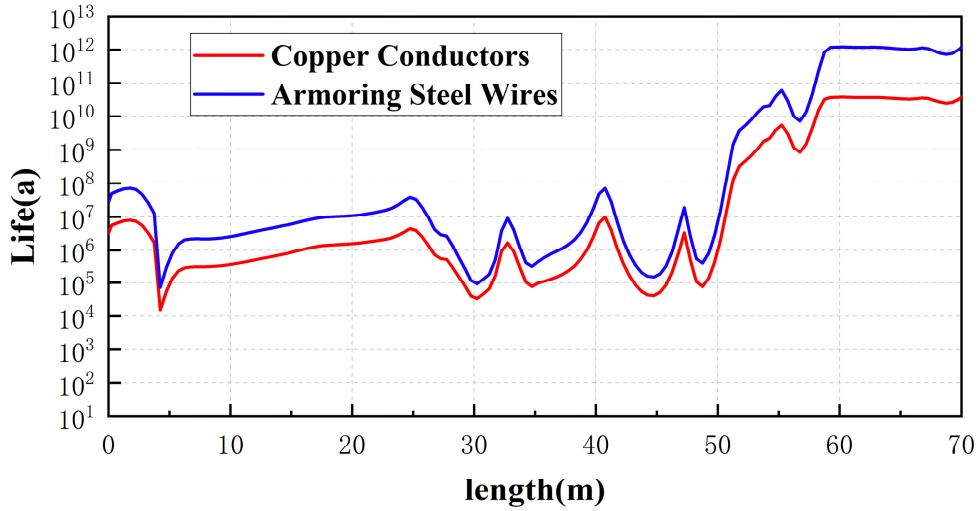

Figure 10. Fatigue results along the cable.

4.3. Discussion

In the same wave height conditions, the cable curvature is maximum under the north-direction waves. This is mainly because the static cable in this study is arranged in the north–south direction. The cable is laid in the sea area with a wave height range of 0–6 m throughout the year. When the wave height is greater than 2 m, the maximum curvature of the cable occurs at the exit of the bend stiffener. Therefore, starting from a wave height of 2 m, with a 1 m interval for wave height values and a wave direction of north, five typical working conditions are defined, namely, Condition 1 to Condition 5. Condition 6 represents an extreme condition that occurs once in a hundred years. Although the frequency of its occurrence is very low, the cable must meet the requirements of extreme conditions. The characteristic parameters of these six typical conditions are shown in Table 8. Fatigue analysis is conducted for the dynamic cable under these conditions, and the curvature, effective tension, and von Mises stress distributions along the cable length are calculated and presented in Figures 11–13, respectively. It can be observed that under the six conditions, the effective tension and von Mises stress of the dynamic cable all satisfy the allowable conditions. However, under Conditions 3 to 6, the curvature of the dynamic cable exceeds the allowable curvature at the bend stiffener exit (4.25 m).

Table 8. Characteristic parameters of typical working conditions.

Working Conditions	Wave Height (m)	Wave Direction
Condition 1	2	N
Condition 2	3	N
Condition 3	4	N
Condition 4	5	N
Condition 5	6	N
Condition 6	11.8	NW

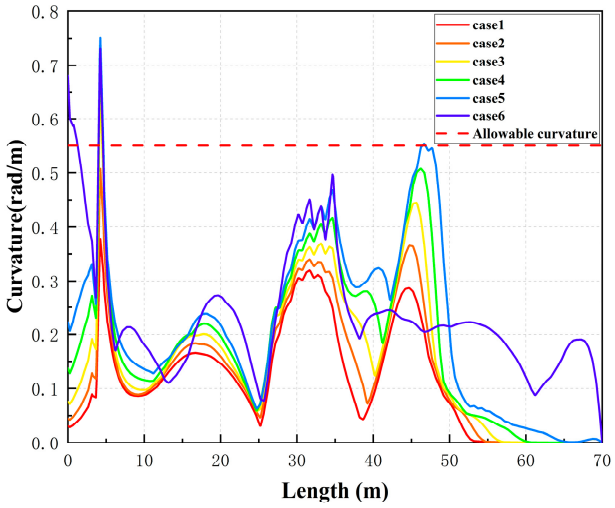

Figure 11. Dynamic cable curvature along the cable length.

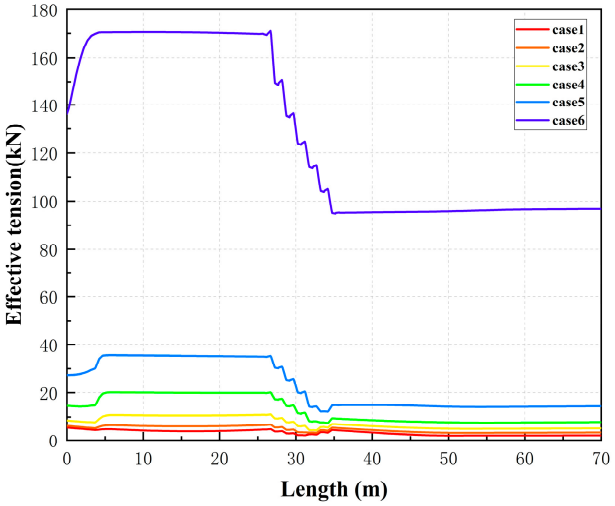

Figure 12. Dynamic cable effective tension along the cable length.

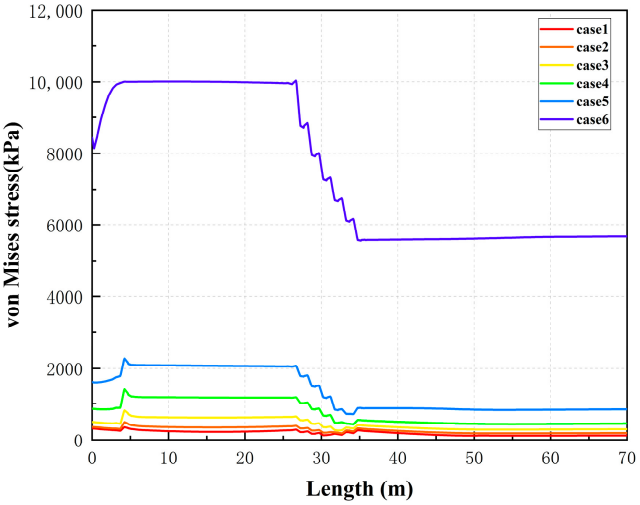

Figure 13. von Mises stress along the cable length.

In order to prevent the curvature of the dynamic cable from exceeding the allowable limit at the exit of the bend stiffener, this study adopts the following preventive measures:

(1) Method I: Drawing inspiration from similar measures used in flexible cables [21], add weight blocks to the section of the dynamic cable exiting the bend stiffener (as shown in Figure 14). The parameters of the weight block are listed in Table 9. The results, depicted in Figure 15, reveal a significant reduction in the curvature of the submarine cable at the exit of the bend stiffener compared to Figure 11. However, under Condition 6, the curvature at the root of the bend stiffener exceeds the allowable limit. The literature [21] suggests that this occurrence may be due to insufficient strength of the bend stiffener. It can be inferred that the addition of the weight block increases the load on the dynamic cable, causing the bend stiffener to lack the necessary strength. To ensure that the curvature of the entire cable is within the allowable range under this condition, further adjustments to the parameters of the weight block are required. Under Condition 5, the curvature in the arched area behind the dynamic cable's float block exceeds the allowable limit. When no weight block is added, the curvature in this area is close to the allowable limit. This indicates that adding the weight block has some influence on the curvature in this area. However, the main factor causing excessive curvature in this area is the float block.

(2) Method II: Changing the hanging angle of the dynamic cable's bend stiffener (as shown in Figure 16), studying the influence of the bend stiffener hanging angle on the maximum curvature, effective tension, and von Mises stress of the dynamic cable under different conditions. Figure 17 shows the distribution of the maximum curvature along the length of the dynamic cable with a hanging angle of 45°. Compared with Figure 11, the curvature of the cable at the bend stiffener outlet is significantly reduced. Therefore, adjusting the hanging angle can effectively reduce the cable curvature. By varying the hanging angle, further research on its impact on the dynamic cable's maximum curvature, effective tension, and von Mises stress is conducted, and the results are shown in Figures 18–20. As the hanging angle of the dynamic cable's bend stiffener increases, the curvature at the bend stiffener outlet gradually decreases under Condition 6, and at 40°, it is lower than the allowable curvature, and in this condition, the dynamic cable's maximum curvature always occurs at the bend stiffener outlet. For Conditions 1 to 5, the curvature at the bend stiffener outlet decreases with the increase in the hanging angle. In working Conditions 1 to 5, when the hanging angle is adjusted to 15°, 20°, 30°, 30°, and 30°, the curvature of the dynamic cable bending preventer is reduced to lower than the curvature of the rest of the dynamic cable, respectively; the maximum curvature of the dynamic cable shifts from the exit of the bend stiffener to the midpoint of the arch behind the buoyancy block. Therefore, there is a maximum value for adjusting the overall maximum curvature of the cable with the hanging angle. Beyond this value, the dynamic cable's maximum curvature shifts from the bend stiffener outlet to the midpoint of the arch after the floating block area, and the effect of adjusting the hanging angle disappears. With the increase in the hanging angle, the maximum effective tension and maximum von Mises stress for each condition gradually increase, but the increase is relatively slow. As indicated in Figures 19 and 20, with the increase in the hanging angle, the maximum effective tension (i.e., the maximum pulling force experienced by the cable during operation) and the maximum von Mises stress of the dynamic cable gradually increase for each working condition, but the magnitude of the increase is relatively moderate. Therefore, applying a certain hanging angle to the dynamic cable can ensure that the cable curvature at the bend stiffener outlet meets the allowable requirements. However, the hanging angle of the bend stiffener should not be too large to avoid ineffective adjustment and unnecessary increases in cable tension and stress.

Table 9. Parameters of the weight block.

Weight Block	Weight/t	Position/m
Weight Block 1	0.3	6
Weight Block 2	0.3	8
Weight Block 3	0.3	10
Weight Block 4	0.3	12
Weight Block 5	0.3	14
Weight Block 6	0.3	16
Weight Block 7	0.3	18

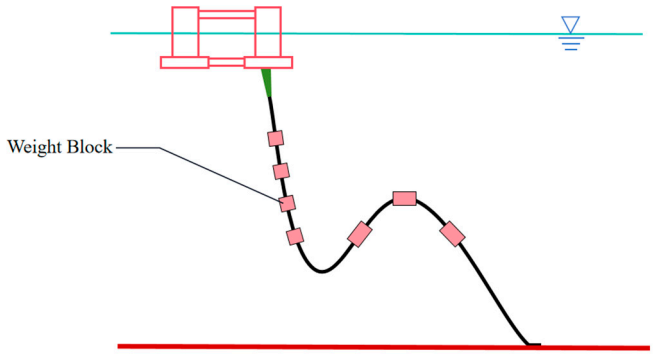

Figure 14. Dynamic cable with added weight blocks.

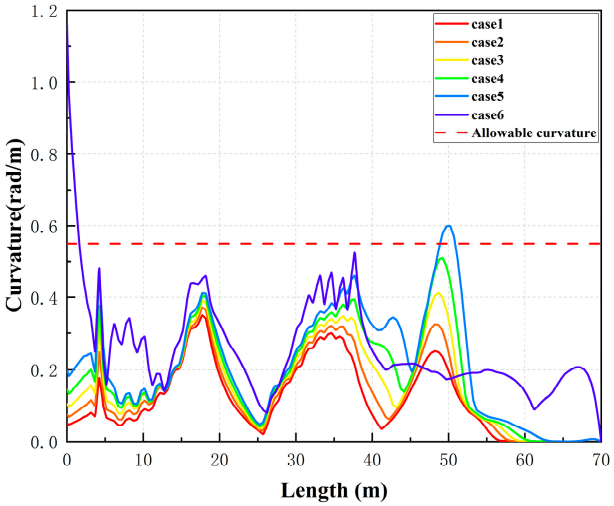

Figure 15. Curvature distribution of dynamic cable after adding weight blocks.

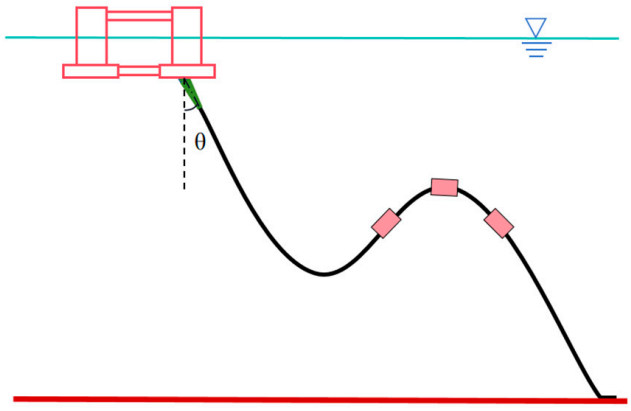

Figure 16. Dynamic cable changing the hanging angle.

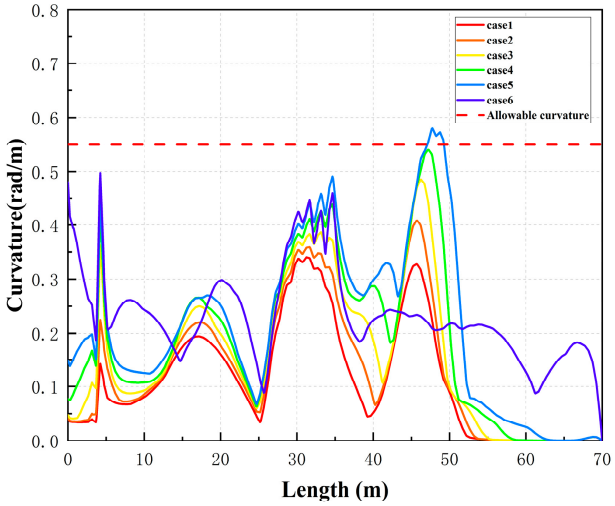

Figure 17. Curvature distribution along the cable length with the hanging angle of 45°.

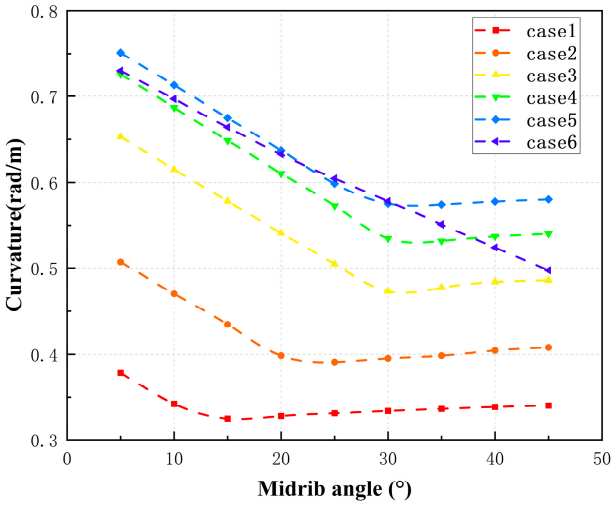

Figure 18. Relationship between hanging angle and maximum curvature.

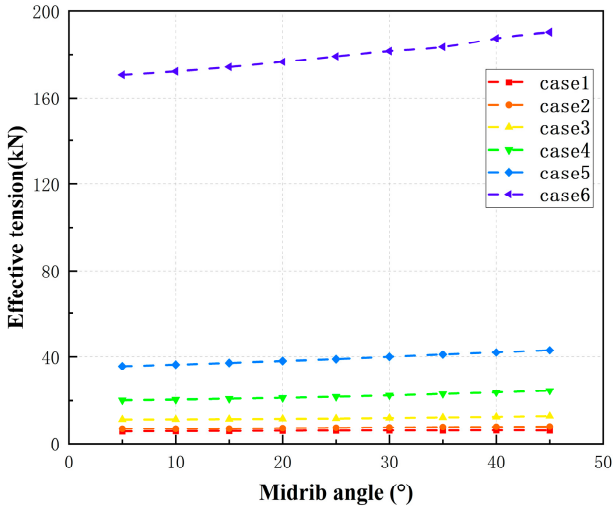

Figure 19. Relationship between hanging angle and maximum effective tension.

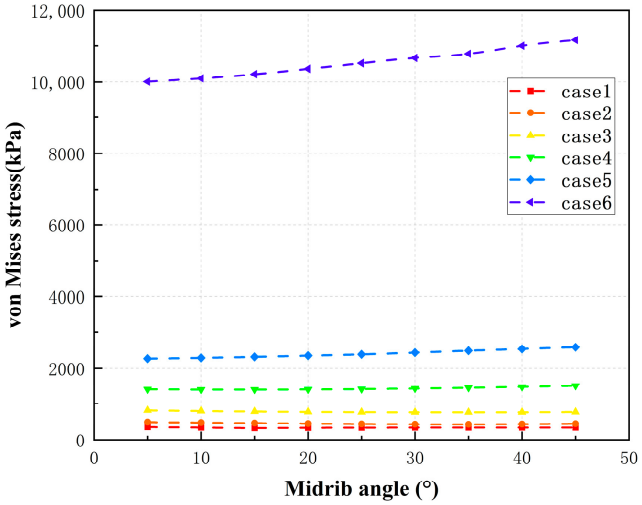

Figure 20. Relationship between hanging angle and maximum von Mises stress.

In comparison between using the method of adding a weight block (Method I) and adjusting the hanging angle to 45° (Method II), the effective tension and von Mises stress of the dynamic cable are shown in Figures 21 and 22. Both methods increase the effective tension and von Mises stress of the dynamic cable from the bend stiffener to the floating block section. However, Method II generates maximum effective tension and maximum von Mises stress that are 45.87% and 45.86% lower, respectively, than those produced by Method I. Therefore, adopting Method II can reduce the stress and tension of the dynamic cable, which is beneficial for extending the cable's lifespan. It can also be observed that when the hanging angle changes, such as from 5 degrees to 45 degrees, the effective tension and von Mises stress of the dynamic cable from the bend stiffener to the floating block section increase, but the magnitude is limited. Therefore, adjusting the hanging angle to reduce curvature while having a minimal impact on effective tension and von Mises stress is feasible for different conditions.

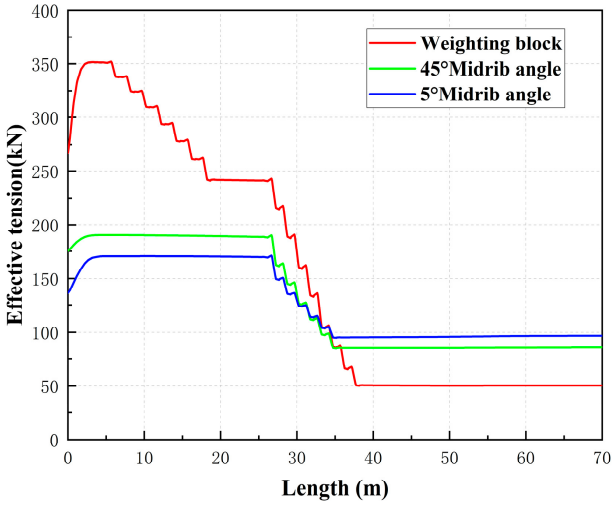

Figure 21. Effective tension of dynamic cable with added weight and hanging angle of 45°.

Compared to the two methods mentioned above, both approaches can ensure that the dynamic cable curvature at the out-of-bend section meets the allowable curvature under different working conditions. In practical engineering, the gravity block is located underwater, making it difficult to adjust according to working conditions. Additionally, adding a gravity block increases the maximum effective tension and von Mises stress of the dynamic cable, which is detrimental to the cable's lifespan and imposes additional

loads on the connection components between the cable and the platform. On the other hand, adjusting the hanging angle can be achieved by designing a bend stiffener with an automatically adjustable angle. This device is smaller and closer to the sea surface, making it more convenient to operate. Furthermore, adjusting the hanging angle does not introduce additional stress loads on the cable, making it more suitable for practical engineering applications.

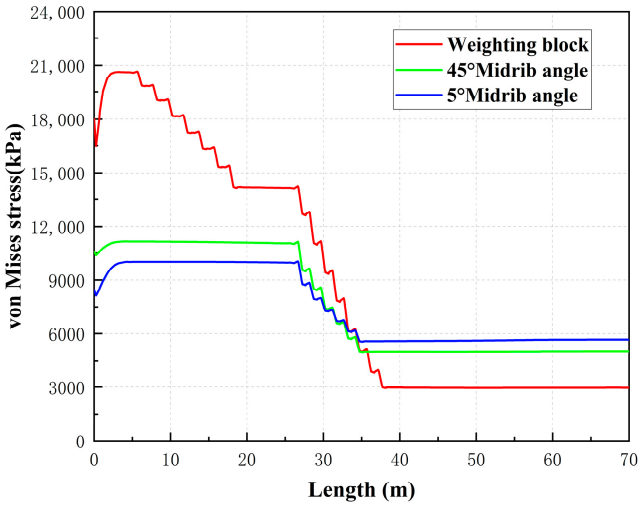

Figure 22. von Mises stress of dynamic cable with added weight and hanging angle of 45°.

5. Conclusions

This paper starts from the actual working conditions of the marine area, conducts a fatigue life assessment of dynamic cables based on the joint probability distribution of multiple operating conditions, and studies methods to reduce the maximum curvature of the cable and thus reduce fatigue damage. The main conclusions are as follows:

(1) The fatigue analysis of the cable indicates that, with a safety factor of 10, the dynamic cable meets the design requirement of a 30-year service life in the studied marine area. The fatigue analysis was conducted under six typical operating conditions corresponding to different wave heights. It was observed that the dynamic cable experiences maximum curvature at the bend stiffener exit. To reduce this curvature, two methods were employed in this study: Method I, involving the addition of a weight block, and Method II, adjusting the hanging angle of the bend stiffener. Both methods effectively reduced the curvature at the bend stiffener exit, leading to increased effective tension and von Mises stress from the bend stiffener to the floating block section. However, the maximum effective tension and von Mises stress generated by Method II were 45.87% and 45.86% lower than those produced by Method I, respectively.

(2) Given the challenges associated with changing the weight block parameters of the dynamic cable in response to different operating conditions, the method proposed in this paper involves adjusting the bend stiffener's hanging angle to reduce the curvature of the dynamic cable. To address varying operating conditions, an automated bend stiffener capable of adjusting its hanging angle according to different scenarios can be designed based on the method proposed in this study. This bend stiffener can be an extension of the existing structure, incorporating a hanging angle adjustment mechanism and an intelligent control system. When facing different operating conditions, especially unexpected extreme conditions, the control system can regulate the hanging angle adjustment mechanism to ensure that the bend stiffener adapts its angle. This ensures that the curvature of the dynamic cable remains within the allowable range, preventing failure due to curvature exceeding permissible limits. Designing such a bend stiffener with automatic hanging angle adjustment presents

several challenges. Firstly, current bend stiffener designs are still limited to traditional fixed types, lacking designs for hanging angle adjustment mechanisms and control systems. Secondly, addressing the energy supply for this bend stiffener is crucial. It can be powered by the floating wind turbine's self-generation capabilities, or an integrated wave energy harvesting device can provide the necessary power. Finally, the response speed of the bend stiffener in adjusting the hanging angle needs to be considered when facing different operating conditions.

Author Contributions: Methodology, Z.G. and Z.W.; Validation, J.L.; Data curation, Z.G.; Writing—original draft, X.Z.; Writing—review & editing, Q.M.; Funding acquisition, Z.G. All authors have read and agreed to the published version of the manuscript.

Funding: This work was financially supported by the Science and Technology Project of POWERCHINA Hainan Electric Power Engineering Co. Ltd. (2023-08).

Institutional Review Board Statement: Not applicable.

Informed Consent Statement: Not applicable.

Data Availability Statement: Data are unavailable due to privacy or ethical restrictions but will be provided when requested.

Conflicts of Interest: Author Zhitao Guo was employed by the company POWERCHINA Hainan Electric Power Engineering Co. Ltd. The remaining authors declare that the research was conducted in the absence of any commercial or financial relationships that could be construed as a potential conflict of interest.

References

1. Liu, Z.; Yu, J.; Huang, D.; Wang, T.; Zheng, Y. Researchon development of offshore wind power. *Ship Eng.* **2020**, *42*, 20–25.
2. Zhou, H.; Hou, C.; Li, H.; Dong, Y. Applicability analysis of floating wind turbine foundation in China. *Wind Energy* **2020**, *7*, 102–105.
3. Gao, K.; Li, C.; Gao, W.; Che, Y. New-type floatingoffshore wind power generation and its key technology research. *Energy Res. Inf.* **2010**, *26*, 110–116.
4. Liu, C.; Xu, Y. Analysis on development prospect offloating offshore wind power in China. *Sino-Glob. Energy* **2020**, *25*, 16–21.
5. Global Wind Energy Council (GWEC). *Global Offshorewind Report 2021 [EB/OL]*; Global Wind Energy Council (GWEC): Brussels, Belgium, 2021.
6. Snazell, Zellers, Eitschun, Neves, Tejeda, Sabrie. *Development of Wet Type AC 66 kV TR-XLPE Insulated Cables[C]//CIGRE Session48*; CIGRE: Paris, France, 2020; p. B1.219.
7. Quest Floating Wind Energy (QFWE). *Global Offshore Windmarket & Forecast Report [EB/OL]*; Quest Floating Wind Energy (QFWE): Sugar Land, TX, USA, 2021.
8. Equinor. *Data Sharing-the Future of Offshore Wind is Afloat [EB/OL]*; Equinor: Singapore, 2021.
9. Zhao, S.; Cheng, Y.; Chen, P.; Nie, Y.; Fan, K. A comparison of two dynamic power cable configurations for a floating offshore wind turbine in shallow water. *AIP Adv.* **2021**, *11*, 035302. [CrossRef]
10. Jiang, J.; Li, Y.; Gou, H. Extreme and fatigue analyses of a dynamic bundled submarine cable. *Ocean Eng. Equip. Technol.* **2020**, *7*, 163–169.
11. Larsen, C.M.; Passano, E. Fatigue life analysis of production risers. In Proceedings of the Annual Offshore Technology Conference, Houston, TX, USA, 27–30 April 1987; pp. 427–437.
12. Hoffman, J.; Dupont, W.; Reynolds, B. A fatigue-life prediction model for metallic tube umbilicals. In Proceedings of the Offshore Technology Conference, Houston, TX, USA, 2–5 May 2001.
13. Sousa, J.R.M.D.; Sousa, F.J.M.D.; Siqueira, M.Q.D.; Sagrilo, L.V.; de Lemos, C.A.D. A theoretical approach to predict the fatigue life of flexible pipes. *J. Appl. Math.* **2012**, *2012*, 983819. [CrossRef]
14. Ruan, W.; Shi, J.; Sun, B.; Qi, K. Study on Fatigue Damage Optimization Mechanism of Deepwater Lazy Wave Risers Based on Multiple Waveform Serial Arrangement. *Ocean Eng.* **2021**, *228*, 108926. [CrossRef]
15. Guo, X.; Nie, Y.; Liu, J.; He, Y.; Mao, L.; Wang, G.; Dai, L. Three-dimensional nonlinear vibration model and fatigue failure mechanism of deepwater test pipe. *Nonlinear Dyn.* **2022**, *108*, 1101–1132. [CrossRef]
16. Lu, H.; Vaz, M.A.; Caire, M. Flexible riser tensile armour stress assessment in the bend stiffener region. *Eng. Struct.* **2022**, *254*, 113849. [CrossRef]
17. Shen, G.; Macdonald, J.; Coules, H. Bending Fatigue Life Evaluation of Bridge Stay Cables. *J. Eng. Mech.* **2022**, *148*, 04021168. [CrossRef]

18. Wokem, C.; Joseph, T.; Curley, M. Fatigue life prediction for cables in cyclic tension. *J. Strain Anal. Eng. Des.* **2018**, *53*, 141–155. [CrossRef]
19. Young, D.; Ng, C.; Oterkus, S.; Li, Q.; Johanning, L. Assessing the mechanical stresses of dynamic cables for floating offshore wind applications. *J. Phys.* **2018**, *1102*, 012016. [CrossRef]
20. Young, D.; Ng, C.; Oterkus, S.; Li, Q.; Johanning, L. Predicting failure of dynamic cables for floating offshore wind. In Proceedings of the 3rd International Conference on Renewable Energies Offshore, Lisbon, Portugal, 8–10 October 2018.
21. Pu, D.; Yang, W.; Feng, R.; Yu, G.; Yang, F.; Chen, R.; Song, Y.; Zhang, Z. Dynamic cable design for shallow water floating wind turbines. *Ocean Eng. Equip. Technol.* **2020**, *7*, 412–418.
22. *API 17B[S]*; Recommend Practice for Flexible Pipe. American Petroleum Institude: Washington, DC, USA, 2014.
23. *IEC 61400-3[S]*; Wind Energy Generation Systems-Part 3-2: Design Requirements for Floating Offshore Wind Turbines. IEC: Geneva, Switzerland, 2019.
24. *DNV-OS-F201[S]*; Dynamic Risers. DNV: Bærum, Norway, 2001.
25. Yuan, Z.; Zou, K.; Sun, Y.; Liu, G.; Qu, Y.; Li, J. Fatigue analysis of dynamic cable based on time domain analysis. *Ocean Eng. Equip. Technol.* **2022**, *9*, 50–55.
26. Nasution, F.P.; Sasvik, S.; Gjosteen, J.K.O. Fatigue Analysis of Copper Conductor for Offshore Wind Turbines by Experimental and FE Method. *Energy Procedia* **2012**, *24*, 271–280. [CrossRef]
27. *DNVGL-RP-C205 [R]*; Environmental Conditions and Environmental Loads. DNVGL: Bærum, Norway, 2017.
28. Veritas, D.N. Fatigue design of offshore steel structures. In *DNV Recommended Practice DNV*; DNV: Bærum, Norway, 2011.